Ab-initio determined electronic and magnetic properties of half-metallic NiCrSi and NiMnSi Heusler alloys; the role of interfaces and defects

I. Galanakis[*]

Department of Materials Science, School of Natural Sciences, University of Patras, GR-26504 Patra, Greece

K. Özdoğan[†]

Department of Physics, Gebze Institute of Technology, Gebze, 41400, Kocaeli, Turkey

E. Şaşıoğlu[‡]

Institut für Festkörperforschung, Forschungszentrum Jülich, D-52425 Jülich, Germany
Fatih University, Physics Department, 34500, Büyükçekmece, İstanbul, Turkey

Using state-of-the-art first-principles calculations we study the properties of the ferromagnetic Heusler compounds NiYSi where Y stands for V, Cr or Mn. NiCrSi and NiMnSi contrary to NiVSi are half-metallic at their equilibrium lattice constant exhibiting integer values of the total spin magnetic moment and thus we concentrate on these two alloys. The minority-spin gap has the same characteristics as for the well-known NiMnSb alloy being around ∼1 eV. Upon tetragonalization the gap is present in the density of states even for expansion or contraction of the out-of-plane lattice parameter by 5%. The Cr-Cr and Mn-Mn interactions make ferromagnetism extremely stable and the Curie temperature exceeds 1000 K for NiMnSi. Surface and interfaces with GaP, ZnS and Si semiconductors are not half-metallic but in the case of NiCrSi the Ni-based contacts present spin-polarization at the Fermi level over 90%. Finally, we show that there are two cases of defects and atomic-swaps. The first-ones which involve the Cr(Mn) and Si atoms induce states at the edges of the gap which persists for a moderate-concentration of defects. Defects involving Ni atoms induce states localized within the gap completely destroying the half-metallicity. Based on single-impurity calculations we associate these states to the symmetry of the crystal.

PACS numbers: 75.47.Np, 71.20.Be, 71.20.Lp

I. INTRODUCTION

Magnetoelectronics, also known as spintronics, is probably the field with the most rapid growth in materials science bringing to the center of scientific research new phenomena.[1,2,3] For researchers dealing with ab-initio calculations one of the most interesting concept in spintronics is the half-metallicity.[4,5,6] Research has been focused initially on the explanation of the origin of the half-metallicity and afterwards on the prediction of new half-metallic materials with potential applications in spintronics devices. Half-metals are hybrids between normal metals and semiconductors: the majority-spin band is crossed by the Fermi level as in a normal metal while the Fermi level falls within a gap in the minority-spin band as in semiconductors leading to a perfect 100% spin-polarization at the Fermi level,[5] maximizing the efficiency of magnetoelectronic devices.[7] de Groot and his collaborators in 1983 were the first to predict the existence of half-metallicity in the case of the intermetallic semi-Heusler alloy NiMnSb,[8] and the origin of the gap seems to be well understood.[9,10,11,12,13,14] There exist several ab-initio calculations on NiMnSb reproducing the initial results of de Groot and collaborators,[15,16,17] and Galanakis *et al.* showed that the gap arises from the hybridization between the *d* orbitals of the Ni and Mn atoms.[9] Moreover in the latter reference it was shown that the total spin moment for the Heusler alloys of the NiMnSb type follows a Slater-Pauling be-

havior being in μ_B the total number of valence electrons in the unit cell minus 18 since there are exactly nine occupied minority-spin states.[9] Theoretical calculations for the interfaces of these materials with the semiconductors are few and all results agree that in general the half-metallicity is lost both at the surfaces[18,19,20,21] and the interfaces with binary semiconductors.[22,23,24,25] Wijs and de Groot have argued than in the case of the NiMnSb/CdS (111) contacts the Sb/S interface keeps half-metallicity when the S atoms sit exactly on top of Sb.[22] Moreover taking into account also the reconstruction at the surfaces and interfaces can have an important effect on their properties.[26] Finally we should note that several other aspects of NiMnSb have been studied using first-principles calculations like the exchange constants and Curie temperatures,[27,28,29] the quasiparticle states[30] and the dynamical effects,[31] the defects and doping,[32,33,34] the structural stability,[35,36] the effect of spin-orbit coupling,[37] the fit of model Hamiltonians to describe NiMnSb,[38,39] orbital magnetism,[40] the pressure and thermal expansion effects,[41] the temperature effect[42] and the magneto-optical properties.[43,44]

The half-metallic character of NiMnSb in single crystals has been well-established experimentally. Infrared absorption[45] and spin-polarized positron-annihilation[46,47] gave a spin-polarization of ∼100% at the Fermi level. High quality films of NiMnSb have been grown,[48,49,50,51,52,53] but they were found not to reproduce the half-metallic character of the bulk. Values of

58% and 50% for the spin-polarization at the Fermi level were obtained by Soulen *et al.*[54] and by Mancoff *et al.*,[55] respectively, and recently Zhu *et al.*[56] found a value of 40% using spin-resolved photoemission measurements on polycrystalline films. Ristoiu *et al.*[57,58,59,60] showed that during the growth of the NiMnSb thin films, Sb atoms segregate to the surface decreasing the obtained spin-polarization; they measured a value of ∼30% at 200K, while at room temperature the net polarization was practically zero. But when they removed the excess of Sb by a flash annealing, they managed to get a nearly stoichiometric ordered alloy surface terminating in MnSb. Inverse photoemission experiments at room temperature revealed that the latter surface shows a spin-polarization of about 67±9% which is significantly higher than all previous values.[58] There is also experimental evidence that for a temperature of ∼80 K there is transition from a half metal to a normal ferromagnet,[61,62] but these experiments are not yet conclusive. Finally, the effect of stress on the magnetic anisotropy of thin NiMnSb films and the role of defects have been explored.[63,64]

Based on the success of first-principles electronic structure calculations to describe the properties of NiMnSb, several authors have predicted new half-metallic Heusler alloys crystallizing in the $C1_b$ structure of semi-Heusler compounds like NiCrM and NiVM (M= P, As, Sb, S, Se and Te),[65,66,67] and XCrAl (X= Fe, Co, Ni) and NiCrZ (Z= Al, Ga, In).[68] Recently, Katayama-Yoshida and collaborators published a paper including also ab-initio calculations on NiMnSi semi-Heusler alloy, which was predicted to have a Curie temperature of 1050 K,[69] exceeding even the 730 K shown by NiMnSb.[70] This finding motivated us to study the electronic and magnetic properties of this compound in detail since except the very high Curie temperature, it should be easily grown due to the well-known and well-controlled growth of NiMnSb and it should be compatible with Si (Si crystallizes in a diamond structure and the unit cell of NiMnSi is two times the unit cell of Si). We decided to expand our study to cover also the closely-related NiCrSi and NiVSi alloys. NiVSi was found not to be half-metallic at its equilibrium lattice constant and thus we focused our study on NiCrSi and NiMnSi alloys. In section II we present the details of our calculations and in section III the electronic and magnetic properties of the bulk phase of these alloys. In section IV we discuss the robustness of half-metallicity and ferromagnetism, and in section V the properties of (100) surfaces and of their interfaces with the Si, GaP and ZnS semiconductors which have an experimental lattice constant almost identical to the theoretical equilibrium lattice constants of NiCrSi and NiMnSi. Finally in section VI we discuss the effect of defects and disorder and in section VII we summarize and conclude.
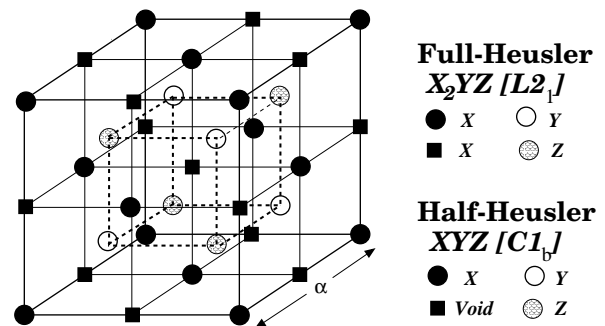

FIG. 1: Schematic representation of the $C1_b$ structure adopted by the semi-(or half-)Heusler compounds like NiMnSi and of the $L2_1$ structure adopted by the full-Heusler compounds like Co_2MnSi. The lattice consists of 4 fcc sublattices. The unit cell in the case of semi-Heuslers XYZ is that of a fcc lattice with four atoms as basis: X at $(0\,0\,0)$, Y at $(\frac{1}{4}\,\frac{1}{4}\,\frac{1}{4})$, a vacant site at $(\frac{1}{2}\,\frac{1}{2}\,\frac{1}{2})$ and Z at $(\frac{3}{4}\,\frac{3}{4}\,\frac{3}{4})$ in Wyckoff coordinates. In the case of full-Heusler compounds the vacant site is also occupied by a X atom.
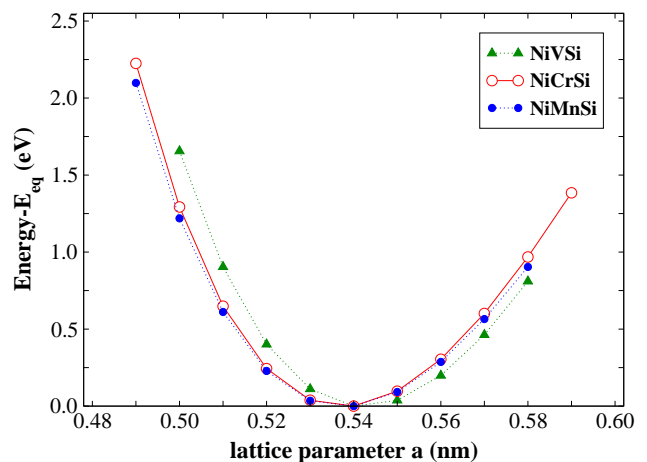

FIG. 2: Calculated total energy within the FPLO method vs the lattice constant. All three compounds have a theoretical equilibrium lattice constant close to 0.54 nm. Note that we have scaled for each compound the total energy so that the zero energy corresponds to the one of the equilibrium lattice constant.

II. DESCRIPTION OF PRESENT CALCULATIONS

To study the NiYSi alloys we have employed both the full–potential nonorthogonal local–orbital minimum–basis band structure scheme (FPLO)[71,72] and the full-potential screened Korringa-Kohn-Rostoker (FSKKR) method.[73,74] Both methods as we will discuss later give similar results for the bulk alloys. FPLO is suitable to study the disorder within the coherent-potential approximation (CPA). FSKKR is suitable to study surfaces and interfaces since its screened character and the use of decimation method for the inversion of the Green function matrix lead to an order N scaling of the CPU
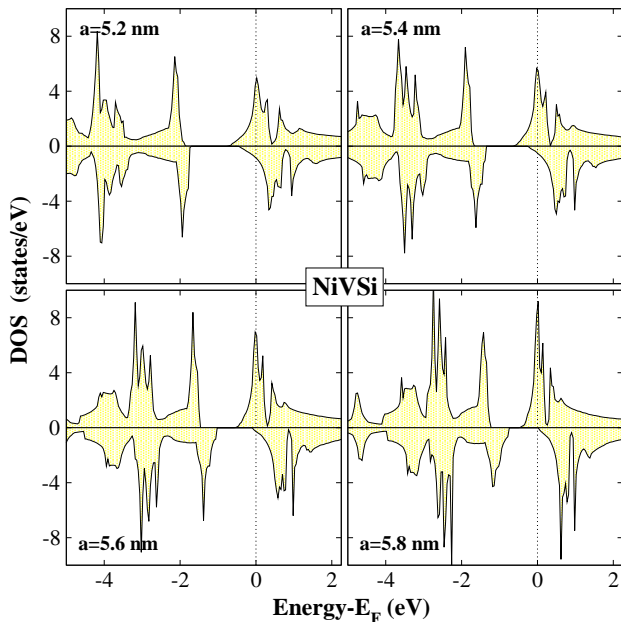
FIG. 3: (Color online)FPLO calculated total density of states (DOS) for the NiVSi compound for four different values of the lattice constant. Positive values of the DOS correspond to the majority (spin-up) electrons and negative values to the minority (spin-down) electrons. The zero of the energy has been chosen as the Fermi energy.

TABLE I: (Color online)Atom-resolved and total spin magnetic moments in μ_B calculated using both the FPLO and FSKKR methods. In the last two columns we present our results on the Curie temperature in Kelvin units calculated with both the mean-field (T_C^{MFA}) and random-phase (T_C^{RPA}) approximations.

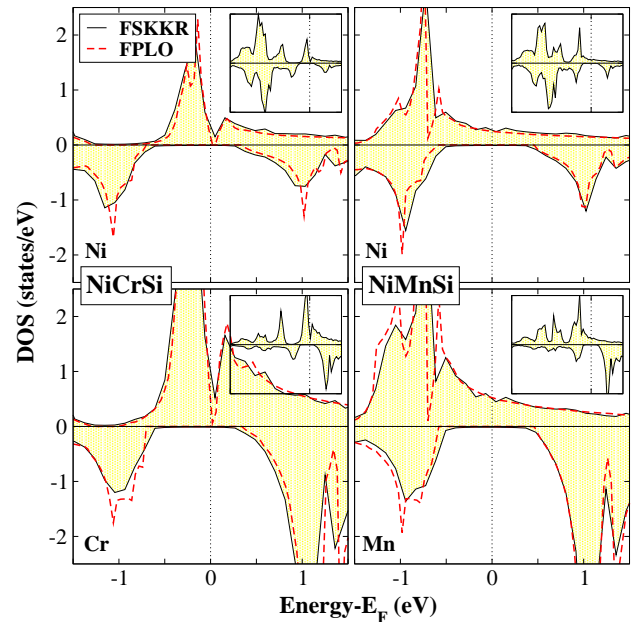| Compound	m^{Ni}	m^Y	m^{Si}	m^{total}	T_C^{MFA}	T_C^{RPA}
NiVSi (FPLO)	0.094	0.791	-0.011	0.874	201	174
NiCrSi (FPLO)	0.127	2.020	-0.148	2.000	900	698
NiCrSi (FSKKR)	0.167	1.858	-0.089	1.969		
NiMnSi (FPLO)	0.207	3.005	-0.212	3.000	1505	1120
NiMnSi (FSKKR)	0.231	2.845	-0.134	2.965		

FIG. 4: (Color online)Ni and Cr(Mn) resolved DOS for both NiCrSi and NiMnSi compounds using both the FPLO and FSKKR methods. In the insets we present the DOS for a wider energy range.

time, where N is the number of inequivalent atoms in the unit cell. Moreover Dyson equation makes possible the study of single impurities within the framework of FSKKR in real space.[75,76] In both cases we employed the local-spin-density approximation (LSDA)[77] for the exchange-correlation energy within the framework of the density functional theory.[78,79]

Semi-Heusler alloys (also known as half-Heusler compounds) crystallize in the $C1_b$ structure which consists of four fcc sublattices and have the chemical formula XYZ where X a high-valent transition metal atom, Y a low-valent transition metal atom and Z a sp atom. In Fig. 1 we present both the $C1_b$ structure of semi-Heuslers and the $L2_1$ structure of the full-Heusler compounds like Co_2MnSi. The unit cell is that of a fcc lattice with four atoms as basis: X atoms occupy the $(0\,0\,0)$ site, Y atoms the $(\frac{1}{4}\frac{1}{4}\frac{1}{4})$, the $(\frac{1}{2}\frac{1}{2}\frac{1}{2})$ site is vacant for the semi-Heuslers and occupied by X in the case of full-Heuslers, and finally Z atoms occupy the $(\frac{3}{4}\frac{3}{4}\frac{3}{4})$ site (we use Wyckoff coordinates to denote the sites). The zinc-blende structure adopted by a large number of semiconductors, like GaP and ZnS is also consisting of four fcc sublattices. In the case of GaP the $(0\,0\,0)$ site is occupied by a Ga atom, the $(\frac{1}{4}\frac{1}{4}\frac{1}{4})$ site by a P atom, while the other two sites are unoccupied. The diamond structure of Si is also coherent with the $C1_b$ structure of semi-Heusler alloys since double the unit cell gives the zinc-blende structure of binary semiconductors. This close structure similarity makes the Heusler alloys compatible with the existing semicon-

ductor technology and thus very attractive for industrial applications.

Since the compounds under study have not been grown experimentally, we have to determine their equilibrium lattice constant. In Fig. 2 we plot the FPLO calculated total energies vs the lattice constant for all three NiVSi, NiCrSi and NiMnSi. We have assumed that all three are ferromagnets (which is confirmed by our calculated exchange constants, at least for NiCrSi and NiMnSi, in section IV). We have scaled the total energy for each compound in a way that the zero of the total energy corresponds to the minimum energy at the theoretical equilibrium lattice constants. All three compounds have an equilibrium lattice constant very close to 5.4 Å. We have decided to use the latter one for all calculations presented in this manuscript.

We should also discuss here the reason that led us to neglect NiVSi from our study. In Fig. 3 we present the

total DOS for NiVSi and for four different lattice constants: 5.2, 5.4, 5.6 and 5.8 nm (we remind here that 1 nm = 10 Å). There is a gap both in the majority and minority spin bands and the Fermi level for the equilibrium lattice constant crosses the conduction minority spin-band and the alloy is not half-metallic. Moreover it is located in a peak of the majority-spin DOS making ferromagnetism unstable and probably the compound prefers to be non-magnetic. The calculated total spin moment presented in Table I is 0.874 μ_B lower than the ideal 1.0 μ_B requested by the Slater-Pauling behavior for half-metallic semi-Heusler alloys.[9] We have not calculated the difference between the non-magnetic and ferromagnetic states since it exceeds the scope of this paper. Although the Fermi shifts lower in energy as we expand the lattice and the compound becomes half-metallic the extremely high majority DOS at the Fermi level persists and ferromagnetism seems to be unstable. The latter argument is also confirmed by the calculated exchange constants presented in Fig. 7. The Ni-V interaction is negligible and the V-V exchange constant between vanadium nearest-neighbors presented in the figure is very weak being 8 times smaller than the Mn-Mn interaction in NiMnSi and thus the tendency to ferromagnetism is not very strong. Also the Curie temperature deduced using these exchange constants is ∼200 K within both the mean-field and random-phase approximations and thus it is considerably smaller than the room temperature at which realistic devices should operate. Since NiVSi is not so interesting for applications with respect to NiCrSi and NiMnSi, we have decided not to include it in the rest of our study.

III.   ELECTRONIC AND MAGNETIC PROPERTIES

We will start our discussion from the electronic and magnetic properties of NiCrSi and NiMnSi establishing also the equivalence between the FPLO and FSKKR methods. In Fig. 4 we present the DOS of the transition-metal atoms Ni and Cr(Mn) since the DOS of Si is negligible within both FPLO (dashed line) and FSKKR (solid line). Both methods give almost the same DOS and the only difference is the intensity of some peaks. Especially concerning the gap (in the right panel we have blown-up the region around the Fermi level) both FPLO and FSKKR give the same gap-width, the same position of the Fermi level with respect to the edges of the gap and the same majority-spin DOS at the Fermi level. In Table I we present also the spin moments using both electronic structure methods. FPLO gives integer values of the total spin moments while FSKKR gives slightly smaller values due to the ℓ summation used in FSKKR. This problem has been extensively discussed in Ref. 80. FSKKR overestimates with respect to FPLO the hybridization between the Ni and Mn d-states. Since FPLO gives a more atomic-like description of the Cr and Mn, it pre-
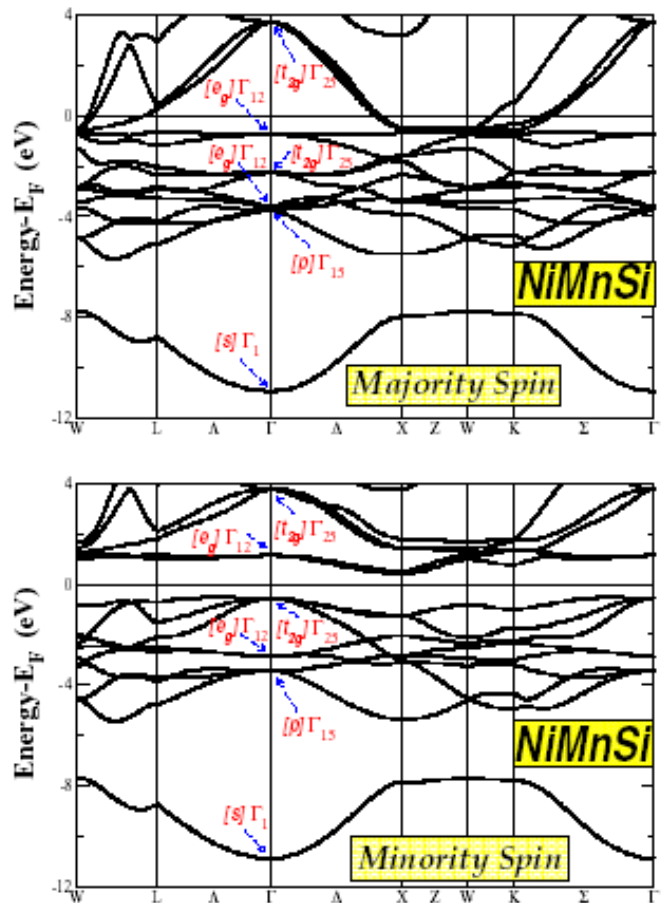

FIG. 5:   (Color online)FSKKR-calculated spin-resolved band structure for the NiMnSi compound along several high-symmetry axis. We have denoted the character of the bands at the Γ point and in the brackets we denote the orbitals transforming following each representation.

dicts larger Cr and Mn spin moments and consequently smaller Ni spin moments to keep constant the total spin moment. Si spin moment shows also a small variation between the two methods since its moment arises from the hybridization with the Ni-Cr(Mn) d hybrids. The total spin moment does not exactly equals the sum of the atomic spin moments of the three constituent atoms since also the vacant site carries a very small spin moment which we do not present in the table.

Since we have established the equilivalence between the FPLO and FSKKR we will go on with the discussion of the electronic and magnetic properties of NiCrSi and NiMnSi. NiMnSi has 21 valence electrons per unit cell, one less than NiMnSb, and NiCrSi 20 valence electrons. In accordance with the Slater-Pauling rule for the perfect half-metallic semi-Heusler compounds presented in Ref. 9 the calculated total spin moment in the unit cell is for NiMnSi 21-18= 3 μ_B and 20-18= 2 μ_B for NiCrSi. The spin moment is mainly carried by the low-valent transition metal atoms Cr and Mn. Ni carries a

TABLE II: (Color online)FPLO calculated width of the minority-spin gap in eV for the cases presented in Fig. 6 with respect to the perfect cubic lattice (the ration equals to zero since $c = a$). Negative values of the ratio in the first column correspond to contraction and positive values to expansion.

$\frac{c-a}{a}$	Gap-Width (eV)	
	NiCrSi	NiMnSi
-5%	1.029	0.966
-2%	1.067	1.050
-1%	1.071	1.055
0%	1.071	1.055
1%	1.021	1.017
2%	0.983	0.987
5%	0.882	0.903

small spin moment of about 0.1-0.2 μ_B due to the hybridization with the Cr(Mn) d-states. Si shows a small spin moment which is antiparallel to the moment of the transition-metal atoms since the majority p-states of Si are more extended in energy and thus partially unoccupied leading to a surplus of minority-spin Si p-states and a negative atomic spin moment.

The origin of the gap is similar to the case of NiMnSb.[9] Ni and Cr(Mn) d-states hybridize creating 5 bonding d hybrids and 5 antibonding ones per spin-direction. Si provides one s- and three p-states per spin low in energy. The p-states accommodate also d electrons of the transition metal atoms. In Fig. 5 we present the band-structure along several high symmetry directions for both spin-directions for NiMnSi. The character of each band at the Γ point reveals the character of the associated orbitals in the real space. First for the minority-spin band structure there is one s and a triple-degenerated at the Γ point p-band coming from the Si atom. Then follow the double-degenerated e_g and triple-degenerated t_{2g} bands due to the Ni-Mn bonding d hybrids. The t_{2g} band is separated by an indirect $\Gamma - X$ gap from the antibonding bands. Thus in total there are exactly nine occupied minority-spin bands. In the majority spin band we have 12 instead of 9 atoms. The two out of the three extra electrons occupy the antibonding e_g states and the last electron occupies partially the antibonding t_{2g} bands. In the case of NiCrSi the majority-spin band has to accommodate 11 electrons and not 12 and thus it is enough to occupy the majority-spin antibonding e_g states. The band associated with the latter states is very narrow and is also well separated in energy from the antibonding t_{2g} bands and this is why in the case of NiCrSi the Fermi level is located in a very narrow deep separating two peaks in the Cr majority-spin DOS.

IV. ROBUSTNESS OF HALF-METALLICITY AND FERROMAGNETISM

We will continue our study discussing the robustness of the half-metalicity and ferromagnetism. Since alloys grow on top of semiconductors, the lattice mismatch can
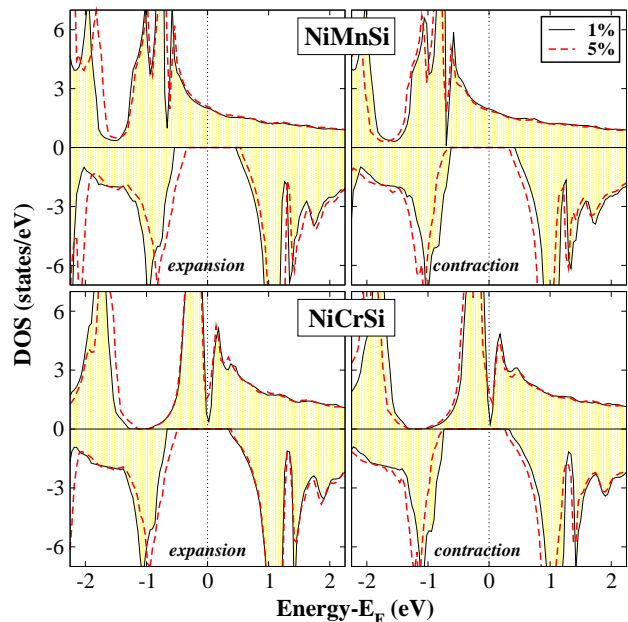

FIG. 6: (Color online)FPLO total DOS of NiCrSi and NiMnSi compounds under 1% and 5% expansion and contraction of the c lattice parameter along the z-axis resulting to a tetragonalization of the lattice. The in-plane lattice parameter was kept constant and equal to 0.54 nm.

lead to a tetragonalization of the lattice of the Heusler alloys to minimize the elastic energy of the film. Thus we have to study for realistic applications the effect of tetragonalization on the half-metallicity. In Fig. 6 we present the total DOS for NiCrSi and NiMnSi using the FPLO code under contraction or expansion of the out-of-plane lattice parameter by 1 and 5% keeping the in-plane lattice constants equal to 0.54 nm. The latter value of tetragonalization is very large and in most realistic applications the lattice relaxes much less. As can been deduced from the figure contraction leads to a marginal shift of the gap while expansion leads to a very small narrowing of the gap. To give more details on the behavior of the gap we present in Table II the width of the gap for the different cases. For the perfect cubic NiCrSi and NiMnSi alloys the gap is 1.071 and 1.055 eV, respectively. Contraction by 5% leads to gap-width of 1.029 and 0.966 eV respectively, while expansion by 5% to 0.882 and 0.903 eV for NiCrSi and NiMnSi respectively. Thus tetragonalization leaves the gap almost unchanged and since for both alloys the Fermi level is near the middle of the gap this has no effect on the half-metallic properties of the two alloys.

Stable half-metallicity does not mean stable ferromagnetism. To study how robust is the ferromagnetism we have to calculate the exchange constants and then use them to calculate the Curie temperature. We have used the formalism presented in Ref. 27 and in Fig. 7 we present the Cr-Cr and Mn-Mn exchange constants as a function of the distance between the atoms. We neglect the Ni-Cr and Ni-Mn interactions since they are very
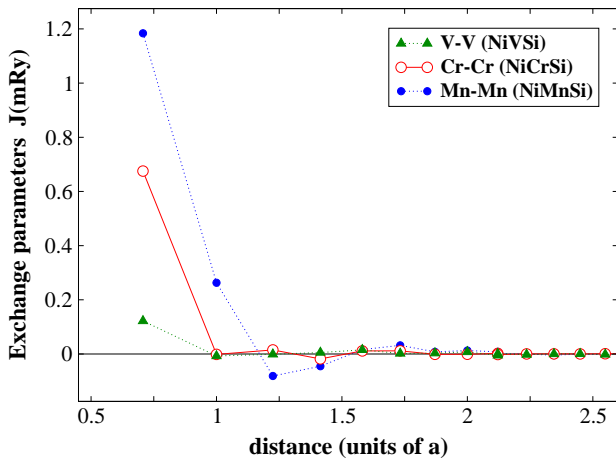
FIG. 7: (Color online)Calculated exchange constants between the low-valent transition metal atoms sitting at the Y site (V, Cr or Mn) as a function of the distance between them.

FIG. 8: (Color online)FSKKR-calculated atom-resolved DOS for the Ni and Cr(Mn) atoms sitting at the first two surface layers for the NiCrSi(001) (left panel) and NiMnSi(001) (right panel) surfaces. Note that e.g. there are two different terminations for the NiCrSi(001) surface: a Ni surface layer with a CrSi subsurface layer or a CrSi surface layer with a Ni subsurface layer.

small even if each Cr or Mn atom has four Ni atoms as first neighbors. The much larger Cr and Mn spin moments are responsible that interactions between them are much larger than between Ni and Cr(Mn) atoms. In the case of NiMnSi the exchange constants are very large and even Mn-Mn next-nearest neighbors contribute to the stability of ferromagnetism. The exchange constant between nearest neighbors, usually in literature denoted as J_1, is 1.2 mRy. This is a very large value and leads to very large values for the Curie temperature (T_C). Calculating the latter one as explained in Ref. 27 we get a value of 1505 K within the mean field approximation (MFA) and 1129 K within the random-phase approximation (RPA) (see Table I) close to the calculated value of 1050 K in Ref. 69. Our experience on NiMnSb shows that the RPA results for semi-Heusler compounds are closer to the experimental values than MFA. In the case of NiCrSi only the interaction between Cr atoms nearest-neighbors contributes to the stability of ferromagnetism and although its strength is smaller than the Mn-Mn one, it is enough to get a Curie temperature as high as 900 K within MFA and 698 K within RPA. Thus both NiCrSi and NiMnSi are very promising for realistic applications since their T_C exceed by far the room temperature of ~300 K.

V. SURFACES AND INTERFACES

A. (001) Surfaces

Although surfaces are not as interesting as interfaces we will start our discussion from the (001) surfaces to give a basis for our discussion in the case of interfaces. We have chosen this surface orientation since this is the most usual one encountered in experiments. We have to note first that we have considered only abrupt surfaces
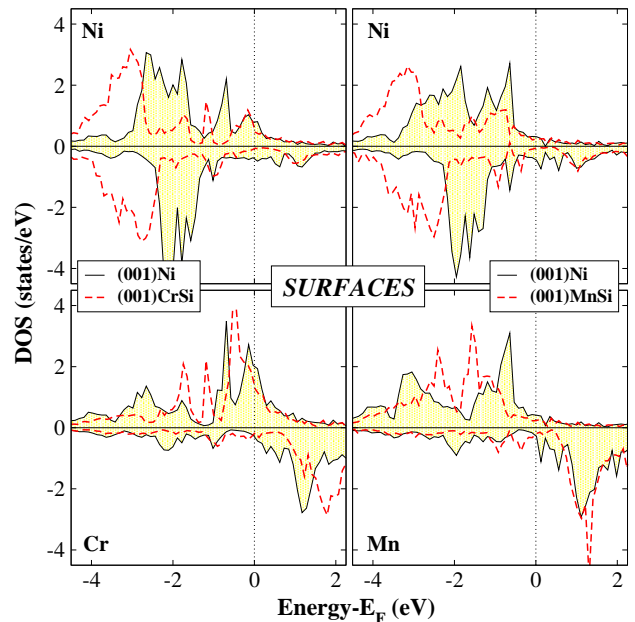
and have not taken into account possible reconstructions. When we open the (001) surfaces in NiCrSi and NiMnSi we have two possible terminations. The surface layer can be either a Ni-Void one with a Cr(Mn)Si as subsurface layer, or vice versa. For the completeness of our results we have considered both terminations and have used a slab of 15 layers embedded in vacuum which has been shown to be adequate for the half-metallic Heusler alloys (see Ref. 19). We have also to note here that the Ni-terminated surfaces contain also a vacant site and are susceptible to show large reconstructions with respect to the CrSi- and MnSi-terminated NiCrSi(001) and NiMnSi(001) surfaces, respectively.[21] Thus we will concentrate mainly on the latter surfaces.

In Fig. 8 we present the DOS of the transition metal atoms at the surface and subsurface layers for both NiCrSi and NiMnSi alloys. It is obvious that in all cases the surfaces are not half-metallic. The bonds which are broken at the surface change the energy position of the states and the gap vanishes similarly to what happens to semiconductors where surface states make their surfaces metallic in most cases. More information we can get from Table III where we present the spin moments of the atoms at the surface and subsurface layers (which are significantly enhanced with respect to the bulk due to the missing hybrization) and also the number of majority ($N^\uparrow$) and minority ($N^\downarrow$) electronic states at the Fermi level for these atoms and the spin-polarization, P,

TABLE III: (Color online)Upper panel: FSKKR calculated atomic spin moments for the NiCrSi(001) and NiMnSi(001) surfaces for both possible terminations. We present the moments for the atoms in the first two surface layers and in the last column their sum. Lower panel: for each one of the atoms in the upper panel we present the ratio of the majority-spin DOS at the Fermi level ($N^\uparrow$) vs the minority-spin DOS at the Fermi level ($N^\downarrow$). In the last column we present the spin-polarization at the Fermi level calculated as $\frac{N^\uparrow}{N^\uparrow+N^\downarrow}$ taking into account both the surface and subsurface layers, P.

	NiMnSi surfaces				
	m^{Ni}	m^{Mn}	m^{Si}	m^{Void}	m^{total}
(001)Ni	0.455	3.166	-0.116	0.037	3.542
(001)MnSi	0.197	3.415	-0.213	0.013	3.412
	NiCrSi surfaces				
	m^{Ni}	m^{Cr}	m^{Si}	m^{Void}	m^{total}
(001)Ni	0.287	2.220	-0.089	0.051	2.439
(001)CrSi	0.091	2.740	-0.180	0.031	2.682

	NiMnSi surfaces				
	Ni ($N^\uparrow/N^\downarrow$)	Mn ($N^\uparrow/N^\downarrow$)	Si ($N^\uparrow/N^\downarrow$)	Void ($N^\uparrow/N^\downarrow$)	P ($\frac{N^\uparrow}{N^\uparrow+N^\downarrow}$)
(001)Ni	0.313/0.453	0.412/0.288	0.131/0.069	0.045/0.049	51%
(001)MnSi	0.242/0.058	0.235/0.191	0.116/0.051	0.043/0.013	67%
	NiCrSi surfaces				
	Ni ($N^\uparrow/N^\downarrow$)	Cr ($N^\uparrow/N^\downarrow$)	Si ($N^\uparrow/N^\downarrow$)	Void ($N^\uparrow/N^\downarrow$)	P ($\frac{N^\uparrow}{N^\uparrow+N^\downarrow}$)
(001)Ni	0.786/0.374	2.045/0.237	0.074/0.024	0.082/0.043	82%
(001)CrSi	0.460/0.063	1.263/0.155	0.083/0.065	0.052/0.015	86%

defined as $\frac{N^\uparrow}{N^\uparrow+N^\downarrow}$ taking into account both the surface and subsurface layers.

We will start our discussion from the CrSi- and MnSi-terminated surfaces. In the case of the CrSi-terminated surfaces the DOS with the exception of the gap area is very similar to the bulk calculations. The Ni atom in the subsurface layer presents practically a half-ferromagnetic character with an almost zero spin-down DOS, while for the bulk NiCrSi there is an absolute gap. The Cr and Si atoms in the surface layer show more pronounced differences with respect to the bulk, and within the gap there is a very small Cr-d DOS. These states are strongly localized at the surface layer as at the subsurface layer there is practically no states inside the gap. When we open the CrSi(001) surface, the Cr atoms at the surface layer loose two out of their four nearest Ni neighbors. This breaking of symmetry at the surface pushes the Cr majority-spin states deeper in energy to account for the missing hybridization and the charge accommodated in these bonds is now accommodated by the Cr majority-spin states leading to a considerable increase of the Cr atomic spin moment as it can be seen also in Table III. Moreover the splitting between the unoccupied Cr states above E_F and the center of the occupied Cr states decreases and at E_F a surface state appears. This behavior of the CrSi-terminated NiCrSi(001) surface is in agreement with previous calculations on the MnSb-terminated NiMnSb(001) surface.[19] Similar is the situation also for the MnSi-terminated NiMnSi(001) surface. Mn atoms act like the Cr ones and accommodate most of the extra-charge due to the broken-bonds in the majority-spin band. But Mn atoms have one valence electron more than Cr atoms which in the bulk is already accommodated in the majority band and thus for Mn atoms the energy cost to accommodate extra charge

in the majority band is larger than for the Cr atoms. As a result part of the extra-charge due to the broken bonds is accommodated also in the minority-spin band leading to a smaller increase of the spin moment with respect to the Cr atoms and a more intense surface state within the gap. Mn atoms at the surface layer show an increase of their spin moment of about 0.6 μ_B with respect to the bulk reaching a value of $\sim$3.4 μ_B, while in the case of Cr atoms the increase of the spin moment with respect to the bulk is 0.9 μ_B.

In the case of the Ni terminated NiMnSi(001) surface, the Ni atoms at the surface layer show a largely different shape of the DOS with respect to the Ni atom at the subsurface layer in the case of the MnSi-terminated surface and the bands are located higher in energy with respect to the MnSi(001) termination. The Mn atoms at the subsurface layer show DOS very similar to the bulk case and the spin magnetic moment is $\sim$3.17 μ_B very close to the bulk value of $\sim$2.84 μ_B. In this case it is clear that there is a minority surface state located exactly at the Fermi level since a very narrow peak centered at the Fermi energy appears in the minority-spin DOS. This surface state survives also for the Mn atoms at the subsurface layer. Similar arguments are also valid for the Ni-terminated NiCrSi(001) surface. Cr atoms behave as in the bulk with slightly larger spin moments. The spin magnetic moment of the Ni atoms at the surface layer is considerable larger than the value for the bulk ($0.28\mu_B$ for the Ni surface atom in NiCrSi with respect to 0.17 μ_B for the Ni atom in the bulk NiCrSi, and $0.46\mu_B$ for the Ni surface atom in NiMnSi with respect to 0.23 μ_B for the Ni atom in the bulk NiMnSi) The surface state in the case of the Ni-terminated NiCrSi(001) surface is more broad than in the case of the NiMnSi alloy and cannot be distinguished from the rest of the DOS.

For applications more important is the spin-polarization at the Fermi level. We present in the lower panel of Table III the number of states at the Fermi level for each atom and for both spin directions. We calculate the spin polarization as the number of majority DOS divided by the total number of electronic states at the Fermi level. In the case of Ni-terminated NiMnSi-surfaces the number of states for the two spin directions is equal due to the surface states and the spin-polarization is around 50% while for the MnSi-terminated surface the surface state is less intense and the spin polarization reaches 67% . In the case of NiCrSi surface Cr atoms show a very large majority-spin DOS at the Fermi level with respect to the Mn atoms since the Fermi level crosses the e_g states. This washes out the weight of the surface states and NiCrSi surfaces show very large values of the spin polarization: 82% for the Ni-terminated surface and 86% for the CrSi-terminated surface. These results do not mean that NiCrSi is more suitable for applications since the electronic properties change considerably at the interfaces with semiconductors.

B. Interfaces

We will continue our study with the interfaces between the half-metal and the semiconductors. Such structures are assumed to present accurately the realistic situation since in most devices half-metals are employed to inject current into a semiconductor. We have assumed that the stacking direction is the (001) and used a slab with 15 layers of the half-metal and 9 layers of the semiconductor in order to have two equivalent interfaces as in Ref. 23. Moreover we have searched for semiconductors crystallizing in the zinc-blende structure which is compatible with the lattice structure of the Heusler alloys[70] and with a lattice constant close to the 5.4Å which is the equilibrium lattice parameter of both NiCrSi and NiMnSi. Such semiconductors are the binary III-V semiconductor GaP, the II-VI semiconductor ZnS and finally the IV semiconductor Si. We have considered all possible interfaces and in Table IV we resume our results by presenting the spin-polarization at the Fermi level taking into account the first two half-metallic interface layers, P_1, and both the first two half-metallic and the first two semiconducting layers, P_2. Note here that contrary to previous studies we define the spin-polarization P as the ratio between the number of majority (spin-up) states and the total number of states at the Fermi level and thus P represent directly the proportion of the majority electrons at the Fermi level. There are two general remarks in this table. First, when we consider also the semiconductor layers the spin-polarization decreases slightly by a few percent in all cases. The interface half-metallic layers polarize the semiconducting layers at their vicinity and the first few semiconducting layers become metallic. But the induced DOS of the semiconductor within the gap is similar for both spin-directions decreasing the spin-
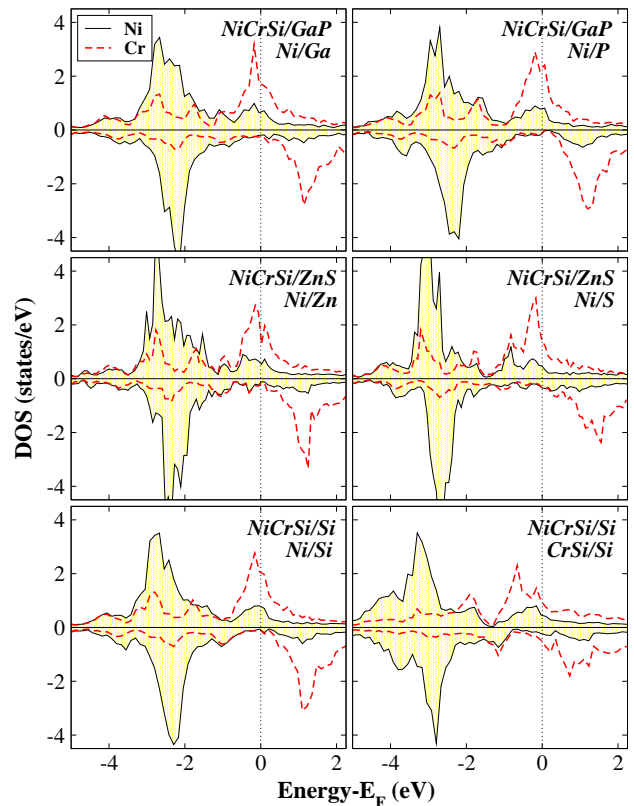

FIG. 9: (Color online)FSKKR-calculated atom-resolved DOS for the Ni and Cr atoms at the interface for the following cases: (i) upper left panel: Ni/Ga structure for the NiCrSi/GaP interface, (ii) upper right panel: Ni/P structure for the NiCrSi/GaP interface, (iii) middle left panel: Ni/Zn structure for the NiCrSi/ZnS interface, (iv) middle right panel: Ni/S structure for the NiCrSi/ZnS interface, (v) lower left panel: Ni/Si structure for the NiCrSi/Si interface, and (vi) lower right panel: CrSi/Si structure for the NiCrSi/Si interface.

polarization. Second, the interfaces between NiMnSi and the three semiconductors show considerably smaller spin-polarization than the corresponding interfaces created by NiCrSi. This is expected since, as for the surfaces, the Cr atoms have a very high majority DOS at the Fermi level with respect to the Mn atoms and they minimize the effect of interface states. Thus in the following we will concentrate on the interfaces between NiCrSi and the three different semiconductors.

When the contact at the interface is created by the Ni atomic layer and not the CrSi layer the obtained spin-polarization is much higher and can exceed 90% as in the case of Ni/P and Ni/Si contacts. The different behavior between the Ni and CrSi interface layers can be easily understood in terms of symmetry and hybridization. Ni interface atoms have a spin moment close to their bulk value as shown in Table V where we present the atomic spin magnetic moments for all atoms at the interface. In the bulk case Ni has 4 Cr and 4 Si atoms as first neighbors. On the Ni-terminated (001) surface the Ni atom loses half of its first neighbors. But if an

TABLE IV: (Color online)Similar to the lower panel of Table III for all studied interfaces between the half-metals NiCrSi and NiMnSi and the GaP, ZnS and Si semiconductors, taking into account all possible interface structures. The spin-polarization ratios at the Fermi level have been calculated as $\frac{N^\uparrow}{N^\uparrow + N^\downarrow}$ taking into account only the two first interface layers of the half-metal, P_1, and the first two interface layers of the half-metal and the first two interface layers of the semiconductor, P_2.

	NiMnSi/GaP Interface			NiCrSi/GaP Interface	
	P_1	P_2		P_1	P_2
Ni/Ga	0.963/0.567 (63%)	1.256/0.800 (61%)	Ni/Ga	2.538/0.569 (82%)	2.771/0.835 (77%)
Ni/P	0.884/0.294 (75%)	1.127/0.462 (71%)	Ni/P	3.212/0.225 (93%)	3.552/0.381 (90%)
MnSi/Ga	0.905/0.810 (53%)	1.156/1.159 (50%)	CrSi/Ga	1.368/0.518 (73%)	1.673/0.766 (69%)
MnSi/P	0.904/1.952 (32%)	1.222/2.575 (32%)	CrSi/P	1.561/0.768 (67%)	1.813/1.037 (64%)
	NiMnSi/ZnS Interface			NiCrSi/ZnS Interface	
	P_1	P_2		P_1	P_2
Ni/Zn	0.868/0.538 (62%)	1.299/0.983 (57%)	Ni/Zn	2.244/0.337 (87%)	2.773/0.690 (80%)
Ni/S	0.796/1.100 (42%)	1.398/1.729 (45%)	Ni/S	2.077/0.878 (70%)	2.747/1.433 (66%)
MnSi/Zn	0.984/1.117 (47%)	1.522/1.724 (47%)	CrSi/Zn	1.563/1.039 (60%)	2.010/1.706 (54%)
MnSi/S	0.761/1.005 (43%)	1.146/1.372 (46%)	CrSi/S	1.903/1.037 (65%)	2.309/1.476 (61%)
	NiMnSi/Si Interface			NiCrSi/Si Interface	
	P_1	P_2		P_1	P_2
Ni/Si	0.993/0.282 (78%)	1.254/0.456 (73%)	Ni/Si	3.016/0.163 (95%)	3.469/0.277 (93%)
MnSi/Si	0.848/1.259 (40%)	1.129/1.854 (38%)	CrSi/Si	1.613/0.866 (65%)	1.873/1.140 (62%)

TABLE V: (Color online)FSKKR calculated atomic spin moments for the two layers of the NiCrSi half-metal and of the two first layers of the GaP, ZnS or Si semiconductors at the interface. $Void$ denotes the empty site in the same layer with the Ni atom. $Vc1$ denotes the empty site in the same layer with Ga(Zn) and $Vc2$ in the same layer with the P(S) atoms. In the case of the interfaces with Si, we denote with Si1 the Si atoms at the interface layer and with Si2 the Si atoms at the subinterface layer.

	NiCrSi/GaP Interface						
	Half-Metal				Semiconductor		
	m^{Ni}	m^{Cr}	m^{Si}	m^{Void}	m^{Ga}	m^{Vc1}	m^{P}	m^{Vc2}
Ni/Ga	0.123	2.050	-0.077	0.046	-0.008	0.031	0.040	-0.003
Ni/P	0.132	2.141	-0.080	0.043	0.005	0.002	-0.031	0.027
CrSi/Ga	0.196	1.873	-0.041	0.037	-0.007	0.053	0.045	0.005
CrSi/P	0.248	2.242	-0.015	0.046	0.031	0.019	0.024	0.077
	NiCrSi/ZnS Interface						
	Half-Metal				Semiconductor		
	m^{Ni}	m^{Cr}	m^{Si}	m^{Void}	m^{Zn}	m^{Vc1}	m^{S}	m^{Vc2}
Ni/Zn	0.118	1.955	-0.087	0.039	-0.012	0.025	-0.001	-0.005
Ni/S	0.256	2.400	-0.064	0.057	0.018	0.004	0.056	0.028
CrSi/Zn	0.177	2.087	-0.067	0.052	0.022	0.035	-0.011	-0.028
CrSi/S	0.168	1.527	-0.035	0.037	0.004	0.004	0.032	0.025
	NiCrSi/Si Interface						
	Half-Metal				Semiconductor		
	m^{Ni}	m^{Cr}	m^{Si}	m^{Void}	m^{Si1}	m^{Vc1}	m^{Si2}	m^{Vc2}
Ni/Si	0.132	2.080	-0.081	0.042	-0.014	0.030	0.025	0.001
CrSi/Si	0.198	1.939	-0.025	0.038	0.005	0.066	0.049	0.013

interface with a semiconductor is formed, the nickels two lost Si neighbors are replaced by two sp atoms presenting similar electronic structure to the Si ones, although they have in general different number of valence electrons, and the situation is much closer to the bulk case than when we have CrSi as an interface layer. Now the Si p bands at lower energy are not destroyed since the sp atoms have a behavior similar to Si and still they accommodate tran-

sition metal d electrons. Thus the only change in the Ni DOS comes from the missing two Cr neighboring atoms. The DOS of the Ni atom at the interface layer presented in Fig. 9 for several Ni/sp contacts is clearly very close to the bulk case. Moreover the Cr atoms at the subinterface layer are also almost bulk like showing with the exception of the gap area a DOS close to the bulk one for all cases of Ni/sp contacts. Between the different cases presented in Fig. 9 -Ni/Ga and Ni/P contacts in the case of NiCrSi/GaP interfaces, Ni/Zn and Ni/S contacts in the case of NiCrSi/ZnS interfaces and Ni/Si contact in the case of NiCrSi/Si interface- the DOS of the Ni interface atoms and Cr subinterface atoms only marginally change. The small variations at the gap area arise from the different hybridization between the t_{2g} d-orbitals of Ni and the p-orbitals of the sp atom which transform with the same representation and thus can couple. When the sp atom is Si the situation is closer to the bulk NiCrSi and we get a P_2 spin polarization as high as 93%. When the sp atom is P which has one electron more than Si the P_2 drops slightly to 90%. As the difference between the electronic structure of Si and the sp atoms becomes more important the hybridization effects become more pronounced inducing a larger DOS in the minority-spin band and thus leading to smaller values of P_2.

In the case when the contact is made up by the CrSi layer the Cr atoms have an immediate environment very different from the bulk NiCrSi and thus their electronic properties are considerably altered with respect to the bulk case. In Fig. 9 we present the DOS of the Cr atom at the interface layer and the Ni atom at the subinterface layer in the case of a CrSi/Si contact. The majority-spin bands are broader with respect to the Ni/Si contact and they are pushed deeper in energy. This attracts some of the minority unoccupied Cr states also deeper in energy and now the Fermi level crosses the antibonding minority d-bands leading to a smaller spin-polarization at the

Fermi level. While the CrSi-based contacts keep a degree of polarization close to 60% due to the large intensity of the Cr majority-spin DOS at the Fermi level, in the case of the MnSi-based contacts the situation is even worse and P_2 becomes smaller than 50% meaning that at the Fermi level the spin-down states are more than the spin-up states.

Finally we should also briefly discuss the spin magnetic moments presented in Table V for the case of NiCrSi/(GaP or ZnS or Si) interfaces. The atoms in the semiconductor spacer become magnetic due to the polarization from the transition-metal atoms in the half-metallic spacer but their spin moments are very small (less than $0.01\mu_B$ in all cases). Ni and Cr atoms in all cases present spin moments close to the bulk values and there is no general trend associating the spin magnetic moments to the spin-polarization of the interfaces. Thus for each case we have to study the DOS at the interface to get valid conclusions about the behavior of the half-metallicity.

We should also note here that we have neglected relaxation effects at the interface. Relaxation effects modify the spin-polarization at the Fermi level since it leads to increased hybridization and charge-transfer. It was shown in the case of a Ni/P contact in the case of the NiMnSb/GaP interface that the Ni-P interlayer distance was reduced by 18%, while the neighboring interlayer distances where expanded by 5-7% as compared to the ideal bulk values leading to a decrease of the spin-polarization.[23] Nevertheless, these effects did not destroy the gap but shifted the local DOS slightly deeper in energy and a suitable doping at the interface restored the spin-polarization. Moreover in the case where the spin-polarization for the unrelaxed surface is as high as 90% as in some of the cases presented above, the effect of relaxation will be much weaker.

VI. DISORDER AND DEFECTS

Our final section is devoted to the effect of defects. Defects in large concentrations can induce new bands within the minority-spin gap and completely destroy half-metallicity. But even in low concentrations they can couple to interface states and the latter ones become conducting destroying the spin polarization during transport experiments through a half-metal/semiconductor interface. To perform our study we have employed the FPLO method within the CPA approximation to account for disorder in a random way. We have studied two types of defects (i) the creations of Mn(Cr) and Si antisites and Mn(Cr)-Si swaps which keep the half-metallic character, and (ii) the creation of Ni antisites and Ni-Mn(Cr) atomic swaps which induce states within the gap destroying the gap.

TABLE VI: (Color online)FPLO calculated width of the minority-spin gap in eV for the cases presented in figure 10 as a function of the disorder concentration x. With "–" we denote the cases where the gap persists but the half-metallicity is lost since the Fermi level is above the gap.

	NiY(Si$_{1-x}$Y$_x$)	
x	Y=Mn	Y=Cr
0	1.055	1.071
0.05	0.584	0.298
0.1	0.437	0.176
0.2	0.206	–
	Ni(Y$_{1-x}$Si$_x$)Si	
x	Y=Mn	Y=Cr
0	1.055	1.071
0.05	0.878	0.878
0.1	0.777	0.773
0.2	0.626	0.613
	Ni(Y$_{1-x}$Si$_x$)(Si$_{1-x}$Y$_x$)	
x	Y=Mn	Y=Cr
0	1.055	1.071
0.05	0.567	0.483
0.1	0.424	–
0.2	0.261	–

A. Defects conserving the half-metallicity

As we have mentioned just above the creation of Cr(Mn) and Si antisites keeps the half-metallic character, as-well-as the Cr(Mn)-Si atomic swaps. The reason is pretty simple. If we examine the band-structure of the minority-spin electrons in Fig. 5 the states just below the gap are the t_{2g} d-hybrids which are mainly located at the Mn(Cr) sites. Above the gap we have the antibonding e_g d-states and then the antibonding t_{2g} d-hybrids. The t_{2g} states transform using the same representation as the p states of the Si atom. The sites occupied by the Si and Cr(Mn) atoms in the perfect compounds have the same symmetry, with four Ni and four Void sites as first neighbors, rotated by 90°. Thus the equivalence between the t_{2g} and p states is obvious. When Cr(Mn) atoms migrate to Si sites or Si atoms to Cr(Mn)sites, it results to a broadening of the bonding t_{2g} hybrids just below the gap. Also the antibonding t_{2g} band above the gap broadens and it overlaps with the antibonding e_g states. These two simultaneous phenomena lead to a shrinking of the gap which as we will discuss below persists for a moderate percentage of disorder. Of course above a critical value of disorder the gap vanishes. In the case of Cr(Mn)-Si atomic swaps, the phenomenon discussed above is more intense and the gap vanishes for a smaller degree of disorder.

In Fig. 10 we present the total, Ni, and Cr(Mn) DOS for the case of 10% Cr(Mn) antisites [NiCr(Si$_{0.9}$Cr$_{0.1}$) and NiMn(Si$_{0.9}$Mn$_{0.1}$) alloys], the case of 10% Si antisites [Ni(Cr$_{0.9}$Si$_{0.1}$)Si and Ni(Mn$_{0.9}$Si$_{0.1}$)Si], and 10% atomic swaps [Ni(Cr$_{0.9}$Si$_{0.1}$)(Si$_{0.9}$Cr$_{0.1}$) and Ni(Mn$_{0.9}$Si$_{0.1}$)(Si$_{0.9}$Mn$_{0.1}$)]. We also present for the first and third case the DOS of the Cr(Mn) impurity atoms
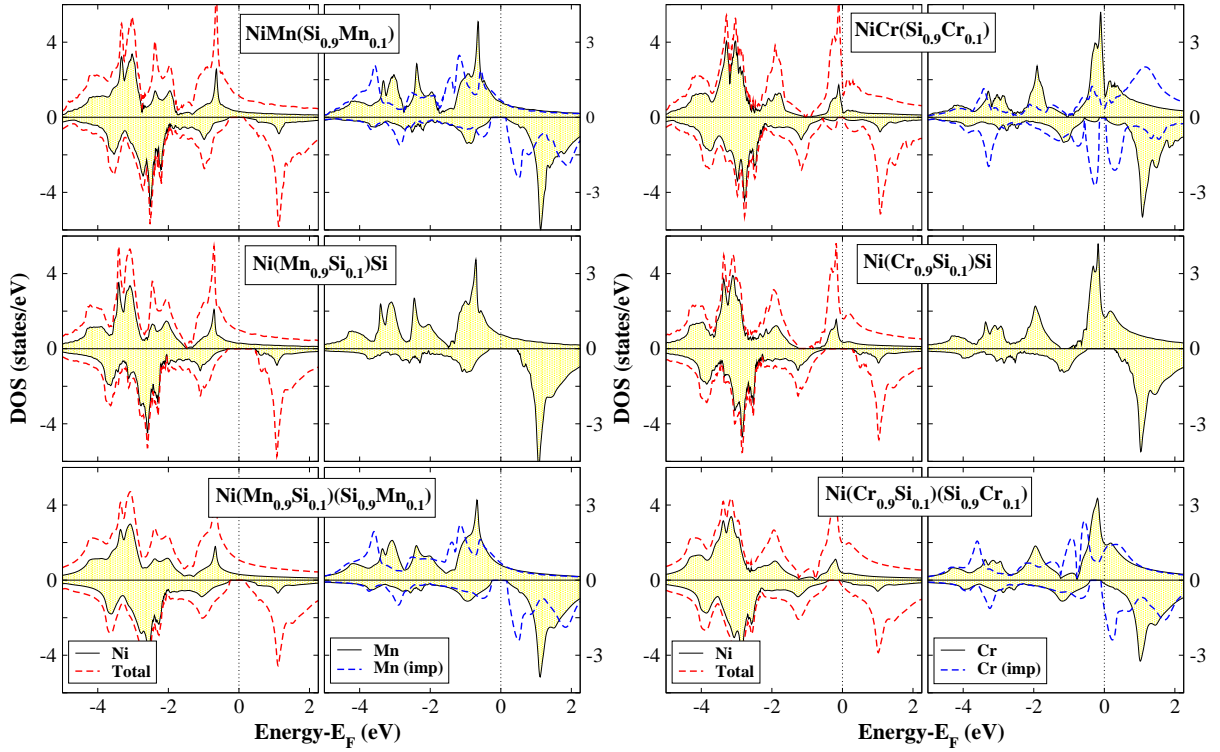
FIG. 10: (Color online)Left panel: FPLO-calculated total and atom resolved DOS for three distinct doping cases in NiMnSi which conserve the half-metallicity. Right panel: similar DOS for NiCrSi. Atomic DOS have been scaled to one atom.

at the antisites. First remark is that Ni DOS is similar for all three compounds and similar to the Ni DOS in the perfect compounds. The same is true for the Cr and Mn atoms at the perfect sites. Thus the antisites and atomic swaps have only marginal effect on the properties of the transition-metal atoms at perfect sites. Concerning now the impurity Cr and Mn atoms sitting at perfect Si sites, the hybridization between the Cr(Mn) t_{2g} states and p states leads to important differences with respect to the Cr and Mn atoms sitting at the perfect sites. The minority-spin impurity states move lower in energy but in the case of the Mn impurities the large exchange splitting between the majority and minority d-states keeps these states well above the gap. In the case of the Cr impurities the exchange splitting is significantly lower than for the Mn impurities and the Cr unoccupied minority e_g states are crossed by the Fermi level in the case of atomic swaps (lower panel). In the case of Cr antisites the antibonding e_g states move even lower in energy and the Fermi level falls within a tiny gap separating the antibonding e_g and t_{2g} states and the Cr impurity atoms have an almost vanishing spin magnetic moment. (We do not present the spin moments of the other atoms since they are very close to the values for the perfect compound.)

To confirm the character of the Cr impurity states we have also employed FSKKR method and have made calculations for a single Cr impurity in NiCrSi and in Fig. 11 we present the d states of Cr antisites at a Si site projected on the e_g and t_{2g} orbitals. For the impurity

calculations we perform the self-consistent calculations for NiCrSi and produce the Green function for the bulk compound.[75,76] Then we consider a cluster of 65 atoms surrounding the Si site embedded in an infinite NiCrSi bulk crystal and calculate the electronic structure of the atoms in this cluster in real space considering a Cr atom at the central Si site. (We have to note here that we have neglected the relaxation of the atomic positions within the cluster due to the impurity atom, which is very tedious computationally, since we expect them to be small due to the high symmetry of the crystal and an extensive study of impurities is out of the scope of the present manuscript.) As we can deduce from the DOS in Fig. 4 the antibonding unoccupied minority d-states have mainly their weight at the Cr site while the bonding occupied minority states at the Ni site. The minority e_g-states of the Cr-impurity are located lower in energy with respect to the Cr atom in the perfect site. Moreover they are located exactly above the Fermi level and are also very localized in energy. The t_{2g} minority states of the Cr-impurity atom form a wider band which starts just at the right edge of the e_g peak and goes very high in energy. In the case of atomic swaps the e_g states move even lower in energy forming this tiny gap. The Cr-impurity atom polarizes slightly the neighboring atoms but the effect very quickly vanishes inside the cluster. As we can deduce from these results on a single impurity in a perfect bulk crystal, which are in very good agreement with the results obtained for a disordered crystal within
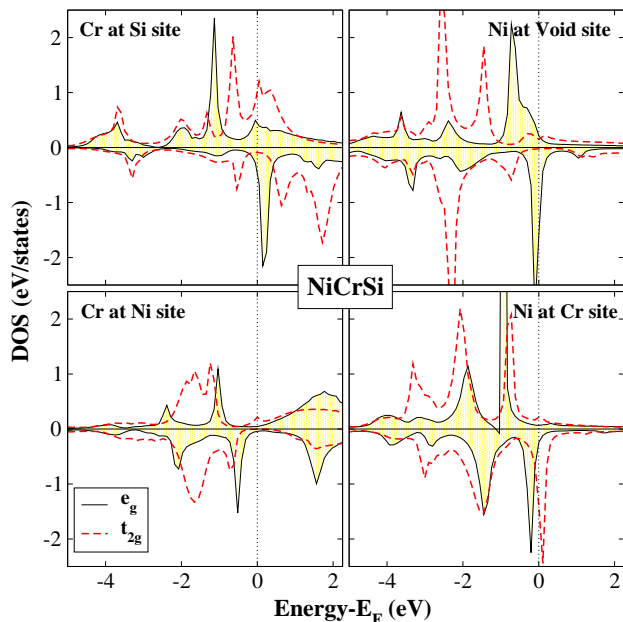
FIG. 11: (Color online)d-resolved atomic DOS for several cases of single impurities in NiCrSi compound calculated using the FSKKR method. The DOS has been decomposed in the double-degenerated e_g and triple-degenerated t_{2g} constituents.
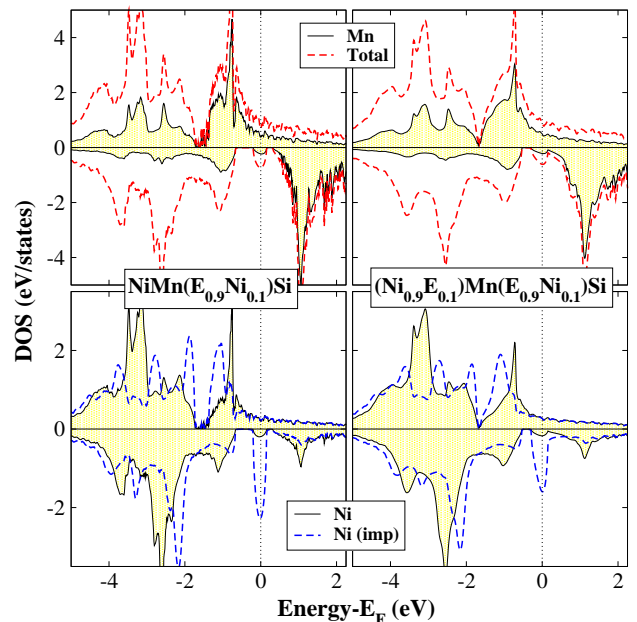

FIG. 12: (Color online)Left panel: FPLO-calculated total and atom resolved DOS for two distinct doping cases in NiMnSi which destroy the half-metallicity. Note that with E we denote the vacant site. Atomic DOS have been scaled to one atom.

the coherent potential approximation (CPA) where each disordered site is occupied by a pseudoatom with mixed Si-Cr properties, local-order effects and long-range effects have the same influence on the electronic properties of NiCrSi alloy. We have performed similar calculations for a single Mn impurity atom sitting at a Si site in NiMnSi and the results were similar to the case of a Cr antisite in NiCrSi but now the e_g and t_{2g} states in the minority-spin band where higher in energy due to the larger exchange-splitting of the Mn occupied majority and unoccupied minority d states.

Finally, we should discuss the width of the gap which is the most interesting property affected by the defects. In table VI we present the width of the gap as a function of the concentration of defects for all three studied cases and for both Cr- and Mn-based compounds. The more mild effect is the creation of Si antisites (middle panel of the table) since no-transition-metal impurities exist. The gap persists with large width-values even for as much as 20% of Si antisites (0.626 eV for the Mn-based compound and 0.613 eV for the Cr-based alloy). When we create atomic swaps (lower panel of the table) the gap-width shrinks with a double rate and for NiMnSi alloys it drops to 0.216 eV for the case of 20% atomic swaps. In the case of NiCrSi the gap-width is half its initial value for 5% of atomic swaps (0.484 eV instead of 1.071 eV). For 10% creation of Cr-Si atomic swaps the gap persists but the Fermi level is above the gap and the defected alloy is not half-metallic. As we have mentioned above in the case of simple Mn(Cr) antisites the gap shrinks very quickly

similarly to what happens for the atomic swaps but in the case of Cr antisites in NiCrSi we have to reach 20% of Cr antisites to loose half-metallicity. Thus for moderate values of antisites and atomic swaps (around 5-10%) both NiCrSi and NiMnSi remain half-metallic although the gap shrinks with respect to the perfect alloys.

B. Defects destroying the half-metallicity

We will proceed now with the case of defects destroying the gap and firstly the creation of Ni antisites at the void site. We have studied two cases (i) there is a surplus of Ni atoms at the void site [NiCr$(E_{1-x}Ni_x)$Si and NiMn$(E_{1-x}Ni_x)$Si compounds where E denotes the void site], and (ii) Ni atoms migrate from the perfect Ni site to the void site conserving the number of Ni atoms [$(Ni_{1-x}E_x)Cr(E_{1-x}Ni_x)$Si and $(Ni_{1-x}E_x)Mn(E_{1-x}Ni_x)$Si compounds]. We present in Fig. 12 the DOS for the Mn-based compounds and for $x = 0.1$ for both kind of Ni antisites. The results are similar for the Cr-based alloys and thus we do not present the DOS in this case. We see than in all cases there is a clear peak instead of the minority-spin gap. This is not present only for the Ni impurity atom but also for the Ni and Mn atoms at the perfect sites. In the case of Ni surplus the intensity of the peak is larger and is more localized in energy. All other details of the DOS are the same with the perfect NiMnSi compound and the Ni impurity atom has a similar DOS with the Ni atoms at the perfect sites
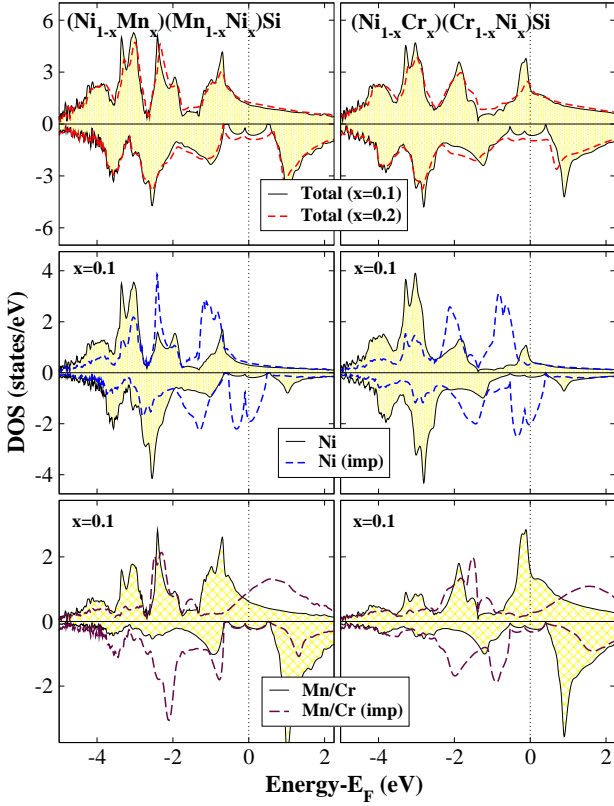
FIG. 13: (Color online)FPLO-calculated total and atom re-
solved DOS for the case of Mn-Ni atomic swaps in NiMnSi
(left panel) and Cr-Ni atomic swaps in NiCrSi (right panel).
Atomic DOS have been scaled to one atom.

TABLE VII: (Color online)FPLO calculated atomic spin mo-
ments in μ_B for the case of Mn-Ni and Cr-Ni atomic swaps in
NiMnSi and NiCrSi compounds, respectively, within the CPA
approximation. In the case of the perfect compounds ($x = 0$)
we give in parenthesis the spin moment of a single impurity
atom calculated using the FSKKR method.

	$(\text{Ni}_{1-x}\text{Mn}_x)(\text{Mn}_{1-x}\text{Ni}_x)\text{Si}$					
x	m^{Ni}	$m^{Ni(imp)}$	m^{Mn}	$m^{Mn(imp)}$	m^{Si}	m^{total}
0	0.207	(0.424)	3.005	(-1.451)	-0.212	3.000
0.1	0.180	0.480	2.849	-1.496	-0.125	2.509
0.2	0.186	0.302	2.674	-1.358	-0.096	1.988
	$(\text{Ni}_{1-x}\text{Cr}_x)(\text{Cr}_{1-x}\text{Ni}_x)\text{Si}$					
x	m^{Ni}	$m^{Ni(imp)}$	m^{Cr}	$m^{Cr(imp)}$	m^{Si}	m^{total}
0	0.127	(0.429)	2.020	(-0.870)	-0.148	2.000
0.1	0.078	0.409	1.652	-0.943	-0.081	1.433
0.2	0.054	0.244	1.196	-0.656	-0.052	0.870

Finally, we have investigated the case of Ni-Cr and Ni-
Mn atomic swaps. These defects have the peculiarity that
Cr(Mn) and Ni atoms move to sites of different symme-
try with respect to their perfect sites in the NiCrSi and
NiMnSi alloys. In Fig. 13 we present for both compounds
the total DOS for two different concentrations of atomic
swaps (x=0.1 and 0.2) and the atom-resolved DOS for
the first case. The Ni and Cr(Mn) atoms at the perfect
sites show a DOS similar to the perfect compounds pre-
sented in Fig. 4. The impurity Ni atoms at the perfect
Cr(Mn) sites show a double-peak structure and the Fermi
level falls within this structure. When the concentration
is increased to 0.2, as it is obvious from the total DOS,
the two peaks overlap creating a wide-band. The Ni im-
purity atoms carry a very large spin moment with respect
to the spin moment of the Ni atoms at the perfect Ni site
as can be seen in Table VII where we present the spin
magnetic moments for both Cr- and Mn-alloys and for
various concentrations of atomic swaps. As we increase
the concentration of atomic swaps the spin moments of
both the Ni impurity atoms and Ni atoms at the perfect
sites decrease. The changes are even more important for
the Cr(Mn) atoms at the Ni sites. Due to the different
symmetry these atoms have a spin moment antiparallel
to the spin moment of the other transition metal atoms
reducing considerably the total spin moment and leading
to ferrimagnetic alloys. This behavior is present also in
the case of Cr and Mn impurity atoms at perfect Co sites
in Co$_2$CrAl(Si) and Co$_2$MnAl(Si) full-Heusler alloys,[81,82]
where Cr(Mn) impurity atoms have spin moments an-
tiparallel to the spin magnetic moment of the other tran-
sition metal atoms. But in these full-Heusler alloys the
half-metallic character is kept contrary to the compounds
under study here. This is due to the Ni impurity atoms
and not to the Cr(Mn) impurity atoms which have a very
small DOS in the minority-spin band which is obviously
a very weak image of the Ni-impurity DOS. To examine
this behavior even further we have plotted in Fig. 11 the
DOS for a single Cr impurity atom at a perfect Ni site
and for a single Ni impurity atom at a perfect Cr site

since the Void and Ni sites have the same symmetry (four
Mn and four Si atoms as first neighbors). This peak is
present also in the case of the NiCrSi alloys and it has the
same shape and intensity. This gives the hint that this
peak comes from only one band. To investigate it further
we show in Fig. 11 also the case of a single Ni impurity
at a Void site in NiCrSi with the FSKKR impurity code
(the details are the same with the case of Cr at Si site in
NiCrSi discussed above). Clearly the peak comes from
the e_g electrons which form a very narrow band and the
Fermi level is located exactly at this peak. Contrary to
the case of a single Cr impurity at a Si site, this peak
is present for all neighboring atoms and survives practi-
cally for most of the atoms of the cluster showing that
the presence of Ni impurity atoms provokes a shift of the
minority unoccupied antibonding e_g band lower in en-
ergy and this band has its weight mainly on the Cr(Mn)
atoms. We have also examined the cases where x= 0.05
and 0.2 for both NiCrSi and NiMnSi and for both kind
of Ni antisites. Even for x=0.05 the peak is present but
now it is more narrow with larger intensity, and as we
increase the concentration of antisites the peak starts to
occupy a larger energy range and its intensity becomes
smaller. Thus we can safely conclude that Ni antisites at
the vacant site completely kill the spin-polarization.

in NiCrSi. In the case of the Cr impurity atom the gap persists and the spin moment is negative (in Table VII we present in parenthesis the spin moment of the single impurity atoms) and close to the values calculated using the FPLO-CPA code. The Ni impurity atoms at the Cr site show a double peak structure at the Fermi level with the e_g states just below the gap and the Fermi level being pinned exactly at the minority t_{2g} peak. Thus due to symmetry reasons the majority d-states of Ni-impurity atoms are completely occupied leading to large spin moments and the Fermi level falls within a double peak-structure leading to a complete destruction of half-metallicity. Thus any kind of Ni defects leads to loss of the half-metallic character.

VII. SUMMARY AND CONCLUSIONS

We have studied using both the full–potential nonorthogonal local–orbital minimum–basis band structure scheme (FPLO) and the full-potential screened Korringa-Kohn-Rostoker (FSKKR) electronic structure methods the electronic, magnetic and gap-related properties of the NiYSi compounds and have expanded our study also to cover the case of surfaces, interfaces with semiconductors and defects. When Y stands for V, the ferromagnetism is not very stable due to the weak V-V interactions and these compounds are not suitable for applications. When Y stands for Cr or Mn, the ferromagnetism is extremely stable leading to very high values of the Curie temperature which is predicted to be ∼700 K for NiCrSi and ∼1100 K for NiMnSi.

Both NiCrSi and NiMnSi are half-metallic at their equilibrium lattice constant with large width of the minority-spin gap (∼1 eV) and integer values of the total spin moment as predicted by the Slater Pauling rule. The gap is created due to the creation of bonding and anti-

bonding d-hybrids in the minority-spin band. The width of the gap is marginally affected upon tetragonalization even when we expand or contract the lattice by 5%.

NiCrSi (001) surfaces present a high spin-polarization at the Fermi level with respect to the NiMnSi alloy due to the large intensity of the Cr majority-spin density of states (DOS) at the Fermi level. In the case of interfaces with semiconductors with similar lattice parameter (GaP, ZnS and Si), Ni-based contacts show larger spin-polarization since Ni atoms at the interface layer have a more bulk-like environment and in the case of NiCrSi interfaces the high Cr-DOS leads to values of the spin-polarization for the Ni-based contacts as high as 90%.

Finally, we have shown that there are two kind of defects. The defects and atomic swaps involving the Cr(Mn) and Si atoms lead to a broadening of the bands and the gap is slowly shrinking and for a critical value of the defects-concentration it disappears. Ni defects on the other hand lead to a shift of the energy-localized e_g states within the gap and these impurity states completely destroy the half-metallicity.

For realistic applications it seems that NiCrSi is more suitable with respect to both NiMnSi studied here and the well-known and widely studied NiMnSb Heusler alloy. Its Curie temperature is smaller than the Mn-based alloys but it is still high-enough for applications exceeding considerably the room temperature. Moreover the large population of Cr majority-spin states at the Fermi level ensures the high-spin polarization at the Fermi level which is needed for the injection of current in semiconductors. Crucial for the operation of devices based on Heusler alloys is the prevention of the creation of Ni defects, since they induce impurity states within the gap which can couple to interface states and completely destroy the spin-polarization of the current injected into the semiconductor.

* Electronic address: galanakis@upatras.gr
† Electronic address: kozdogan@gyte.edu.tr
‡ Electronic address: e.sasioglu@fz-juelich.de
[1] I. Žutić, J. Fabian, and S. Das Sarma, Rev. Mod. Phys. **76**, 323 (2004).
[2] C. Felser, G. H. Fecher, and B. Balke, Angew. Chem. Int. Ed. **46**, 668 (2007).
[3] H. Zabel, Materials Today **9**, 42 (2006).
[4] Half-metallic alloys: fundamentals and applications, Eds.: I. Galanakis and P. H. Dederichs, Lecture notes in Physics vol. 676 (Berlin Heidelberg: Springer 2005).
[5] I. Galanakis, Ph. Mavropoulos, and P. H. Dederichs, J. Phys. D: Appl. Phys. **39**, 765 (2006).
[6] I. Galanakis and Ph. Mavropoulos, J. Phys.: Cond. Matter **19**, 315213 (2007).
[7] S. A. Wolf, D. D. Awschalom, R. A. Buhrman, J. M. Daughton, S. von Molnár, M. L. Roukes, A. Y. Chtchelkanova, and D. M. Treger, Science **294**, 1488 (2001).
[8] R. A. de Groot. F. M. Mueller, P. G. van Engen, and K.

H. J. Buschow, Phys. Rev. Lett. **50**, 2024 (1983).
[9] I. Galanakis, P. H. Dederichs, and N. Papanikolaou, Phys. Rev. B **66**, 134428 (2002).
[10] D. Jung, H.-J. Koo, and M.-H. Whangbo, J. Mol. Struct. (Theochem) **527**, 113 (2000).
[11] B. R. K. Nanda and S. Dasgupta, J. Phys.: Condens. Matter **15**, 7307 (2003).
[12] B. R. K. Nanda and S. Dasgupta, Comp. Mat. Science **36**, 96 (2006).
[13] L. Offernes, P. Ravindran, and A. Kjekshus, J. All. Comp. **439**, 37 (2007).
[14] J. Kohler, S. Q. Deng, C. Lee, and M. H. Whangbo, Inorganic Chenmistry **46**, 1957 (2007).
[15] E. Kulatov and I. I. Mazin, J. Phys.: Condens. Matter **2**, 343 (1990).
[16] S. V. Halilov and E. T. Kulatov, J. Phys.: Condens. Matter **3**, 6363 (1991).
[17] S. J. Youn and B. I. Min, Phys. Rev. B **51**, 10436 (1995).
[18] M. Ležaic, I. Galanakis, G. Bihlmayer, and S. Blügel, J.

Phys.: Condens. Matter **17**, 3121 (2005).

[19] I. Galanakis, J. Phys.: Condens. Matter **14**, 6329 (2002).

[20] I. Galanakis, J. Magn. Magn. Mater. **288**, 411 (2005).

[21] S. J. Jenkins, Phys. Rev. B **70**, 245401 (2004); S. J. Jenkins and D. A. King, Surf. Sci. **494**, L793 (2001).

[22] G. A. Wijs and R. A. de Groot, Phys. Rev. B **64**, *R*020402 (2001).

[23] I. Galanakis, M. Ležaić, G. Bihlmayer, and S. Blügel, Phys. Rev. B **71**, 214431 (2005).

[24] A. Debernardi, M. Peressi, and A. Baldereschi, Mat. Sci. Eng. C-Bio S **23**, 743 (2003).; ibid., Comp. Mat. Science **33**, 263 (2005).

[25] M. Ležaić, Ph. Mavropoulos, G. Bihlmayer, and S. Blügel, J. Phys. D: Appl. Phys. **39**, 797 (2006).

[26] S. J. Hashemifar, P. Kratzer, and M. Scheffler, Phys. Rev. Lett. **94**, 096402 (2005).

[27] E. Şaşıoğlu, L. M. Sandratskii, P. Bruno, and I. Galanakis, Phys. Rev. B **72**, 184415 (2005).

[28] E. Şaşıoğlu, L. M. Sandratskii, and P. Bruno, Appl. Phys. Lett. **89**, 222508 (2006).

[29] E. Şaşıoğlu, L. M. Sandratskii, and P. Bruno, Phys. REv. B **77**, 064417 (2008)

[30] L. Chioncel, M. I. Katsnelson, R. A. de Groot, and A. I. Lichtenstein, Phys. Rev. B **68**, 144425 (2003).

[31] L. Chioncel, E. Arrigoni, M. I. Katsnelson, and A. I. Lichtenstein, Phys. Rev. Lett. **96**, 137203 (2006).

[32] D. Orgassa, H. Fujiwara, T. C. Schulthess, and W. H. Butler, Phys. Rev. B **60**, 13237 (1999)

[33] B. Alling, S. Shallcross, and I. A. Abrikosov, Phys. Rev. B **73**, 064418 (2006)

[34] J. J. Attema, C. M. Fang, L. Chioncel, G. A. de Wijs, A. I. Lichtenstein, and R. A. de Groot, J. Phys.: Condens. Matter **16**, S5517 (2004).

[35] P. Larson, S. D. Mahanti, and M. G. Kanatzidis, Phys. Rev. B **62**, 12 574 (2000).

[36] T. Block, M. J. Carey, B. A. Gurney, and O. Jepsen, Phys. Rev. B **70**, 205114 (2004).

[37] Ph. Mavropoulos, K. Sato, R. Zeller, P. H. Dederichs, V. Popescu, and H. Ebert, Phys. Rev. B **69**, 054424 (2004).

[38] L. M. Sandratskii, R. Singer, and E. Şaşıoğlu, Phys. Rev. B **76**, 184406 (2007).

[39] A. Yamasaki, L. Chioncel, A. I. Lichtenstein, and O. K. Andersen, Phys. Rev. B **74**, 024419 (2006).

[40] I. Galanakis, Phys. Rev. B **71**, 012413 (2005).

[41] M. Pugaczowa-Michalska, Sol. St. Commun. **140**, 251 (2006)

[42] J. J. Attema, G. A. Wijs and R. A. de Groot, J. Phys.: Condens. Matter **19**, 315212 (2007).

[43] V. N. Antonov, P. M. Oppeneer, A. N. Yaresko, A. Ya. Perlov, and T. Kraft, Phys. Rev. B **56**, 13012 (1997).

[44] I. Galanakis, S. Ostanin, M. Alouani, H. Dreyssé, and J. M. Wills, Phys. Rev. B **61**, 4093 (2000).

[45] M. N. Kirillova, A. A. Makhnev, E. I. Shreder, V. P. Dyakina, and N. B. Gorina, Phys. Stat. Sol. (b) **187**, 231 (1995).

[46] K. E. H. M. Hanssen and P. E. Mijnarends, Phys. Rev. B **34**, 5009 (1990).

[47] K. E. H. M. Hanssen, P. E. Mijnarends, L. P. L. M. Rabou, and K. H. J. Buschow, Phys. Rev. B **42**, 1533 (1990).

[48] W. van Roy, J. de Boeck, B. Brijs, and G. Borghs, Appl. Phys. Lett. **77**, 4190 (2000).

[49] J.-P. Schlomka, M. Tolan, and W. Press, Appl. Phys. Lett. **76**, 2005 (2000).

[50] W. van Roy, M. Wojcik, E. Jedryka, S. Nadolski, D. Jalabert, B. Brijs, G. Borghs, and J. De Boeck, Appl. Phys.

[51] Lett. **83**, 4214 (2003).

[51] J. Giapintzakis, C. Grigorescu, A. Klini, A. Manousaki, V. Zorba, J. Androulakis, Z. Viskadourakis, and C. Fotakis; Appl. Phys. Lett. **80**, 2716 (2002).

[52] S. Gardelis, J. Androulaki, P. Migiakis, J. Giapintzakis, S. K. Clowes, Y. Bugoslavsky, W. R. Branford, Y. Miyoshi, and L. F. Cohen, J. Appl. Phys. **95**, 8063 (2004).

[53] S. Gardelis, J. Androulakis, J. Giapintzakis, O. Monnereau, and P. D. Buckle, Appl. Phys. Lett. **85**, 3178 (2004).

[54] R. J. Soulen Jr. *et al.*, Science **282**, 85 (1998); J.-H. Park, E. Vescovo, H.-J Kim, C. Kwon, R. Ramesh, and T. Venkatesan, Nature **392**, 794 (1998).

[55] F. B. Mancoff, B. M. Clemens, E. J. Singley, and D. N. Basov, Phys. Rev. B **60**, *R*12 565 (1999).

[56] W. Zhu, B. Sinkovic, E. Vescovo, C. Tanaka, and J. S. Moodera, Phys. Rev. B **64**, *R*060403 (2001).

[57] C. N. Borca, D. Ristoiu, H.-K. Jeong, T. Komesu, A. N. Caruso, J. Pierre, L. Ranno, J. P. Nozières, and P. A. Dowben, J. Phys.: Condens. Matter **19**, 315211 (2007).

[58] D. Ristoiu, J. P. Nozières, C. N. Borca, T. Komesu, H.-K. Jeong, and P. A. Dowben, Europhys. Lett. **49**, 624 (2000).

[59] D. Ristoiu, J. P. Nozières, C. N. Borca, B. Borca, and P. A. Dowben, Appl. Phys. Lett. **76**, 2349 (2000).

[60] T. Komesu, C. N. Borca, H.-K. Jeong, P. A. Dowben, D.Ristoiu, J. P. Nozières, Sh. Stadler, and Y. U. Idzerda, Phys. Lett. A **273**, 245 (2000).

[61] C. Hordequin, D. Ristoiu, L. Ranno, and J. Pierre, Eur. Phys. J. B **16**, 287 (2000).

[62] C. N. Borca, T. Komesu, H.-K. Jeong, P. A. Dowben, D. Ristoiu, Ch. Hordequin, J. P. Nozières, J. Pierre, Sh. Stadler, and Y. U. Idzerda, Phys. Rev. B **64**, 052409 (2001).

[63] L. Nowicki, A. Turos, A. Stonert, F. Garrido, L. W. Molenkamp, P/ Bach, G. Schmidt, G. Karczewski, and A. Mücklich, Nucl. Instr. and Meth. in Phys. Res. B **240**, 356 (2005).

[64] B. Botters, F. Giesen, J. Podbielski, P. Bach, G. Schmidt G, L. W¿ Molenkamp, and D. Grundler, Appl. Phys. Lett. **89**, 242505 (2006).

[65] M. Zhang, X. Dai, H. Hu, G. Liu, Y. Cui, Z. Liu, J. Chen, J. Wang, and G. Wu, J. Phys: Condens. Matter **15**, 7891 (2003).

[66] M. Zhang, Z. Liu, H. Hu, G. Liu, Y. Cui, G. Wu, E. Brück, F. R. de Boer, and Y. Li, J. Appl. Phys. **95**, 7219 (2004).

[67] E. Şaşıoğlu, L. M. Sandratskii, and P. Bruno, J. Appl. Phys. **98**, 063523 (2005).

[68] H. Luo, Z. Zhu, G. Liu, S. Xu, G. Wu, H. Liu, J. Qu, and Y. Li, Physica B **403**, 200 (2008).

[69] H. Katayama-Yoshida, T. Fukushima, V. A. Dinh, and K. Sato, Jpn. J. Appl. Phys. **46**, L777 (2007).

[70] P. J. Webster and K. R. A. Ziebeck, in *Alloys and Compounds of d-Elements with Main Group Elements. Part 2.*, edited by H. R. J. Wijn, Landolt-Boörnstein, New Series, Group III, Vol. 19/c (Springer-Verlag, Berlin 1988).

[71] K. Koepernik, B. Velicky, R. Hayn, and H. Eschrig, Phys. Rev. B **58**, 6944 (1998).

[72] K. Koepernik and H. Eschrig, Phys. Rev. B **59**, 3174 (1999)

[73] N. Papanikolaou, R. Zeller, and P. H. Dederichs, J. Phys.: Condens. Matter **14**, 2799 (2002).

[74] R. Zeller, J. Phys.: Condens. Matter **20**, 035220 (2008).

[75] T. Korhonen, A. Settels, N. Papanikolaou, R. Zeller, and P. H. Dederichs, Phys. Rev. B **62**, 452 (2000).

[76] N. Papanikolaou, B. Nonas, S. Heinze, R. Zeller, and P. H.

Dederichs, Phys. Rev. B **62**, 11118 (2000).

[77] S. H. Vosko, L. Wilk, and N. Nusair, Can. J. Phys. **58**, 1200 (1980).

[78] P, Hohenberg and W. Kohn, Phys. Rev. **136**, B864 (1964).

[79] W. Kohn and L. J. Sham, Phys. Rev. **140**, A1133 (1965).

[80] I. Galanakis, P. H. Dederichs, and N. Papanikolaou, Phys. Rev. B **66**, 174429 (2002).

[81] K. Özdoğan, I. Galanakis, E. Şaşıoğlu, and B. Aktaş, Phys. Stat. Sol. (RRL) **1**, 95 (2007).

[82] K. Özdoğan K, I. Galanakis, E. Şaşıoğlu, and B. Aktaş, Sol. St. Commun. **142**, 492 (2007).